Thermo Electron Engineering Corporation, 85 First Avenue, Waltham, Massachusetts 02154

Report No. TE 41-64

THIRD QUARTERLY REPORT
FOR
SURFACE AND ADSORBATE STUDIES

September 25, 1963, to December 25, 1963

by

D. Lieb
S. S. Kitrilakis
J. H. Weinstein

Contract No. NAS 3-2539

Prepared for

National Aeronautics and Space Administration
Lewis Research Center
21000 Brookpark Road
Cleveland 35, Ohio

Thermo Electron Engineering Corporation, 85 First Avenue, Waltham, Massachusetts 02154

Report No. TE 41-64

THIRD QUARTERLY REPORT
FOR
SURFACE AND ADSORBATE STUDIES

September 25, 1963, to December 25, 1963

by

D. Lieb
S. S. Kitrilakis
J. H. Weinstein

Contract No. NAS 3-2539

Technical Management
NASA-Lewis Research Center
Nuclear Power Technology Branch
Gerald R. Brendel

Approved by: S. Kitrilakis
S. S. Kitrilakis
Research Manager

TABLE OF CONTENTS

PRECEDING PAGE BLANK NOT FILMED.

LIST OF FIGURES

CHAPTER I
INTRODUCTION

This program is concerned with experimental studies of the emission characteristics of monocrystalline and polycrystalline thermionic converter electrode materials. The effects of cesium and cesium fluoride environments upon the work function distribution of the surface, under various conditions of coverage, is the major area of interest. Another variable is the type of surface preparation given the surface.

The experimental work makes use of scanners which are unique in that they allow scanning to be performed on surfaces which are in equilibrium with the cesium vapor environment. Two types of scanners have been developed at Thermo Electron. One is a photoelectric scanner suitable for low temperatures where thermionic currents are small. The other is a thermionic scanner for high surface and cesium reservoir temperatures where thermionic currents are significant.

One scanner of each type was fabricated for this program after design changes had been made to accommodate the addition of the reservoir required to contain the additives.

During the third quarter, thermionic scanning of surfaces, in the presence of cesium fluoride, was carried out. Temperature ranges corresponding to both emitter and collector operating conditions were studied in both steady-state and transient operation.

CHAPTER II
SUMMARY

A. Special pulsing circuitry was designed and fabricated which allows testing over a wider range of emitter temperatures by eliminating or minimizing the problem of emitter temperature runaway at high currents.

B. Thermionic scanning of a ⟨110⟩ tungsten surface in a cesium-only environment was accomplished. Both photographic maps and cross scans were recorded for various coverages.

C. Thermionic scanning of the ⟨110⟩ tungsten surface in a cesium-plus-cesium-fluoride atmosphere was accomplished. Again, cross scans, as well as photographic maps, were made.

D. A series of transient tests were conducted to confirm the results discovered during the initial tests with the cesium fluoride environment in the scanner.

During the Third Quarter, more than 200 runs were conducted at various parametric settings. Quantitative work function distributions as a function of cesium and cesium fluoride coverage are being calculated from this data and will appear in the Final Report of this program.

CHAPTER III
PROGRESS DURING THE QUARTER

GENERAL

The investigation of the effects of cesium fluoride in thermionic converters was carried out during this period through the use of the thermionic scanner. Temperature ranges corresponding to both emitter and collector operating conditions were studied. Results from tests with constant additive pressure have been correlated based on the Rasor theory that the T/T_R ratio will uniquely relate to the work function of the test surface. T in this case is the surface temperature, and T_R is the cesium reservoir temperature.

The initial experiments were made in a cesium-only environment. Approximately 75 cross scans at different surface temperatures were made with reservoir temperatures of 375°K, 425°K, and 475°K. Six different lines across the test surface were chosen for these scans. The primary purpose of this work was establishing a reference condition with which to compare the additive results. These experiments also served to define the most favorable operating accelerating field and collector temperature. In addition, about 20 photographs of the displayed patterns were taken to determine the correlation of surface patterns with the cross scans and with the effects of the main magnetic field.

For the second series of experiments, the cesium fluoride additive was allowed to enter the scanner. These tests were made with cesium reservoir temperatures of 425°K and 475°K and with additive reservoir temperatures of 515°K and 615°K. For each set of temperatures approximately 20 cross scans at various surface temperatures were plotted. During this time, the resolution of cross scans was improved by slowing the plotting rate. Two lines across the

test surface were scanned at this slower rate. These results, together with previous experience on the photoelectric scanner and with the additive converter, indicated that an additional soaking period was necessary for the additive to attain its maximum effect.

Further experiments were, therefore, conducted with an overnight soaking period. Another set of 20 scans was made under these conditions. In these tests, time delay effects in the adsorption and desorption of the additive on the test surface became apparent, and a preliminary investigation of this phenomenon was made.

THERMIONIC SCANNER SET-UP

The construction of the test vehicle for the thermionic scanner, incorporating a tungsten emitter and cesium fluoride additive, was described in Report No. TE 29-64. This device has been completed. Outgassing proceeded successfully, and the tube was mounted on a base plate for testing.

Figure 1 is a photograph of the device and mounting hardware. Visible in this figure are: the emitter output lead, emitter radiator, body shell, sapphire window, probe connection and cooling strap, collector heater, additive reservoir, and the base plate. Thermocouples protected by ceramic tubes are provided for measurement and control of the probe, additive, cesium, shell, and emitter temperatures. The base plate supports the tube and contains leadthroughs for all the wires except the emitter output lead, which has been brought through the top to minimize the diameter of the upper section of the tube.

One of the important considerations in the design of the scanner was maximizing the magnetic fields available for deflection and collimation. Since the fields fall off very rapidly with distance, it is desirable to keep the tube and

collimating coil diameter small so that the deflection system may be placed close to the active tube area. A compact coil structure was achieved by using water cooling for all coils. The main collimating field is generated by a flattened copper tubing wound around the upper Vycor. The turns near the window have been spread to provide a clear view. Figure 2 shows the device under vacuum with the deflection coils in place. They are potted in epoxy to ensure mechanical rigidity and connected in orthogonal pairs to provide a rectangular scanning pattern. Each coil is composed of two windings of flattened copper tubing, with parallel water feeds and series electrical connection. The discharge in the tube is observed through the central hole in one of these coils.

INSTRUMENTATION

In the scanner, if useful results are to be obtained, the current reaching the collector and probe must be emission limited and independent of any space charge effects. An accelerating electric field is therefore applied to saturate the discharge. Because of the wide spacing in this tube, and the further increase in effective spacing at large deflection angles, an unusually high voltage is needed. Near the minimum work function conditions, where the tube currents become large, considerable power is dissipated in the discharge. This power finally appears as heat on the emitting surface, causing temperature instability. The problem is particularly severe in the range studied here because of the low temperatures involved and the resulting low values of heat input.

A reduction in the average power dissipated in discharge may be achieved through a pulse technique. If the accelerating field is pulsed to the saturation value with a low duty cycle source, the heating effect will be reduced and the currents will still be emission-limited during a short period sufficient for measurement purposes. Since the fast sweep in the scanner occurs at the line

frequency, a sampling method must be used to slow the effective speed for proper operation of an X-Y recorder. By synchronizing the sampling pulse with the accelerating pulse and varying the phase of the two pulses with respect to the 60-cycle line, a complete plot of a cross scan from the X-Y recorder can be obtained. Figure 3 shows the I-V curve of the tube and indicates the pulse voltages. The curve is entirely in the power-absorbing quadrant because of the wide spacing. Figure 4 illustrates the pulse and sample timing.

The accelerating pulse period corresponds to the 60-cycle sweep frequency so that ignition always occurs at the same value of magnetic field. A delay of 0.8 millisecond between the start of the accelerating pulse and the sample time is provided to allow the discharge to stabilize and any turn-on transients to decay. The sampling pulse opens the sampling gate for a period of about 50 microseconds to record the sweep field and probe current at that time.

Figure 5 shows a typical cross scan as it appears on the oscilloscope. The vertical sweep in the figure is derived directly from the 60-cycle deflection coil voltage, while the horizontal signal is obtained from the probe current. During the interval between accelerating field pulses, only spurious currents such as those emitted from the main collector reach the probe, and the resulting base line forms a zero reference. When the main discharge is ignited, the current from the test surface reaches the probe and appears as the current pedestal in the photograph.

A schematic of the instrumentation is shown in Figure 6. A General Radio 1217B Pulser, synchronized to the line frequency through an adjustable phase shifter, provides the primary pulse source. This source drives the accelerating voltage gate and also triggers the sampling gates in the "waveform translator" through a trigger generator. X and Y signals for the recorder are taken through

the sampling gates from the sweep and from the amplified probe current. Oscilloscopes monitor the tube voltage and cross scan signals. One interesting aspect of the pulsing is its strobing effect on the discharge, which renders the high-speed sweeping action visible through the sapphire window.

TESTING

Introduction

The thermionic scanner examines the work function distribution of a test surface by evaluating, on a point-by-point basis, the characteristics of the current emitted from the heated surface. A qualitative representation of the patterns on the surface is given by brightness in the display picture. Such a picture is produced by scanning the test screen and display screen simultaneously in two orthogonal directions, and intensity-modulating the display in proportion to the current intercepted at the probe. Several patterns are shown in Figures 7 through 10 for various cesium, additive, and surface temperatures. The concentric rings in some of the pictures are due to plasma effects appearing as horizontal striations.

Quantitative data is determined from the currents received during single line scans across the surface. A few typical cross scans are shown in Figures 11 through 14. With a collection of similar cross scans for a given set of fluoride and cesium pressures, and different surface temperatures, the T/T_R dependence of work function may be calculated.

Typical Calculation

To illustrate the procedure, a curve of T/T_R vs ϕ (Rasor Plot) will be plotted. Figure 11 shows several different cross scans of the $\langle 110 \rangle$ tungsten surface temperature of 1060°K, a cesium reservoir temperature of 425°K and

no additive present. Let us choose point "A" on cross scan "0". The relative current at point A is the amplitude of the curve at that point and is 71 graphical divisions. The calibrating current, which is identified graphically as the number of divisions between the two lines marked "Calibration" in Figure 11, has been previously determined to be 0.65 μa. Thus the actual current at point "A" can be calculated. Dividing by the known area of the collector hole (4.6×10^{-5} cm^2) gives the current density through the hole. Repeating this procedure for cross scans covering a range of surface temperatures gives the values shown in Table I. The surface temperature and current density substituted into the Richardson equation give the effective work function of the cesiated surface. These results are plotted in Figure 15. Similar plots were made for different additive and cesium reservoir temperatures.

Test Procedure

Control of vapor pressure in the test vehicle by means of reservoir temperature adjustment necessitates maintaining all the other elements in the device at higher temperatures. Because the additive reservoir is operated hotter than the cesium reservoir, a small orifice in the cesium tubulation is used to block the low-pressure additive vapor from the relatively cold cesium reservoir. However, this same orifice restricts the flow of the cesium vapor and slows the attainment of equilibrium conditions. For this reason, most runs were with a constant reservoir temperature and changing surface temperature. The first runs with cesium only had the additive capsule sealed as described in the previous report on the photoelectric scanner. For additive runs the capsule was cracked and the additive reservoir heated. In some cases at the higher additive temperature the collector had to be cooled below the additive temperature to reduce stray currents from the collector to the probe. The extreme slowness of the additive

response, as described below, restricted the loss of additive pressure during the time necessary to take a set of cross scans.

Analysis of Results

Figures 7 through 10 illustrate the changes in surface patterns as surface temperature and additive pressures are varied. At a surface temperature (T) of 1280° K and a cesium temperature (T_R) of 425° K, the work function is comparatively uniform, as seen in Figure 7. When the additive is introduced, the central region shifts to a significantly higher work function, as shown by the darker shadow in Figure 8. At higher additive pressure (Figure 9), this shift is more pronounced and the area more restricted. It should also be noted that, at lower surface temperatures, where the Rasor Plots for different bare-surface work function values approach each other, the patterns are much more uniform. This may be observed by comparing Figure 10 with Figure 8.

Figure 16 shows ϕ vs T/T_R plots taken at 425° K cesium and several additive temperatures. A similar plot is shown in Figure 17 for 475° K cesium. These runs were all taken with only a short soaking period of about 3 hours at operating temperatures. Under these conditions the effects of the additive were quite small. Another run was therefore made after a 16-hour soak at additive temperature. During this period the emitter was maintained at a low temperature (870° K) and only heated during the run.

The additive curves of Figure 18 compare this data with the cesium-only condition. The additive has now caused a pronounced shift in the position of the minimum work function to lower T/T_R values.

It will be observed that the two additive curves do not coincide. This leads us to conclude that, when the additive is present, the correlation between ϕ and T/T_R is no longer unique.

At any given value of T/T_R the emitter temperature is higher for the curve with the higher value of T_R. Consequently, the additive adsorbed on the test surface will be less for the higher-temperature surface. This leads to the tentative conclusion that, even with constant additive pressure, the value of ϕ will be a function not only of T/T_R but also of another variable which is probably T/T_A. Considerable additional work is required to confirm this tentative conclusion.

In the cross scan of Figure 12 and the display picture, Figure 9, there is a significant difference in the emission properties of the outer region (location B, for example) and that of the central one (location C). Figure 19 demonstrates the behavior of these two patches over the range of surface temperatures. At large T/T_R, the work functions are well separated. As the minimum is approached these lines cross and begin to separate in the reverse order. The bare work functions of these regions are indicated on the plot by the straight lines corresponding to the Rasor curves at high surface temperature.

Time Effects

In addition to the long induction period for the cesium fluoride noted above, there was a shorter transient effect evident whenever the surface temperature was increased. Figure 20 illustrates this effect. Starting at 930° K and T/T_R of 2.2, cross scans were taken at successively lower surface temperatures until the value of T/T_R for minimum work function was passed. About 15 minutes was allowed at each point to stabilize the readings. This data is presented as points 192 to 197. After soaking at the last point (745° K) for 30 minutes, the surface was rapidly heated to 880° K and a cross scan (point 198) taken. As the surface soaked at this temperature, the current gradually decreased. This corresponds to the work function increase indicated by the dotted line to point 200, which is the steady-state value reached after 30 minutes.

The time characteristics of the test surface depend upon the particular region of the surface, as is evident in the cross scans of Figures 12, 13 and 14. All had about 1100° K surface temperature and represent portions of a time cycle. The original scan, Figure 12, was taken after a prolonged soaking to achieve equilibrium. The surface was then cooled slowly to 750° K while taking other scans. Rapid reheating to 1100° K produced the cross scan of Figure 13. In this scan the pronounced dip apparent in Figure 12 has disappeared. After soaking at this temperature for about 30 minutes, the scan in Figure 14 was obtained. The dip has now returned. This evidence indicates a significantly different response between the central and the outer portions of the surface.

TABLE I

Cross Scan No.	T °K	T_R °K	T/T_R	Current Ampl. Div.	Cal. Ampl. Div.	Rel. Ampl.	J $\frac{amp}{cm^2}$	ϕ volts
61	800	425	1.88	20	44	0.455	.006	1.60
59	855	425	2.02	160	12	13.3	.174	1.48
57	930	425	2.19	244	13	18.8	.245	1.58
55	1060	425	2.52	71	13	5.46	.071	1.96
53	1200	425	2.84	30	45	0.666	.009	2.45

CHAPTER IV
PLANS FOR THE FOURTH QUARTER

1. The study of the time effects using cesium fluoride on the tungsten surface will be completed.
2. The molybdenum test surface will be removed from the photoelectric scanner. It will be photographed and examined in the metallography laboratory and prepared for insertion in the thermionic scanner. After reassembly of the thermionic scanner, mapping of the molybdenum surface will be accomplished, first in a cesium-only atmosphere and then in the cesium-plus-cesium-fluoride atmosphere.
3. All data will be reduced and the final report will be prepared.

64-R-2-1

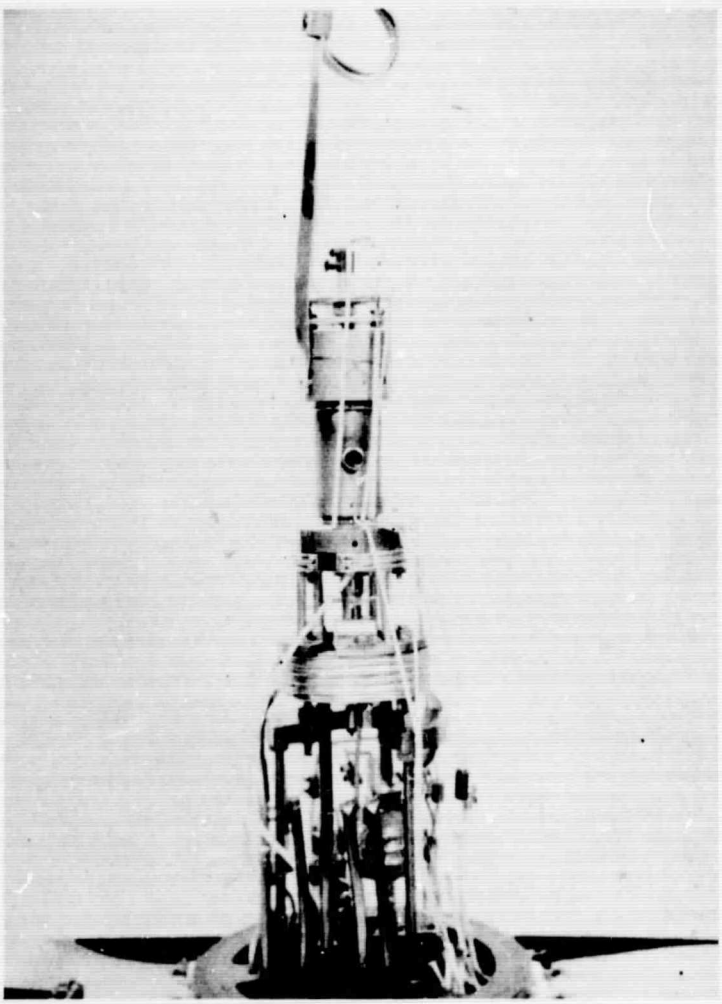

Figure 1. Thermionic Scanner on Stand

64-R-2-2

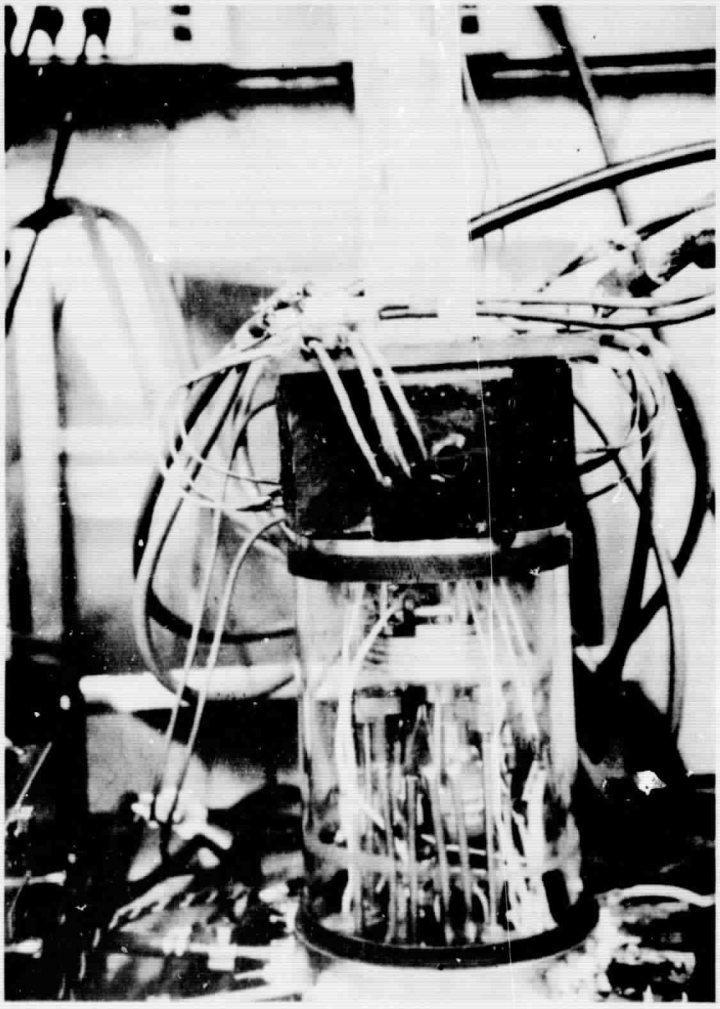

Figure 2. Scanner Under Vacuum With Coils

64-R-2-4

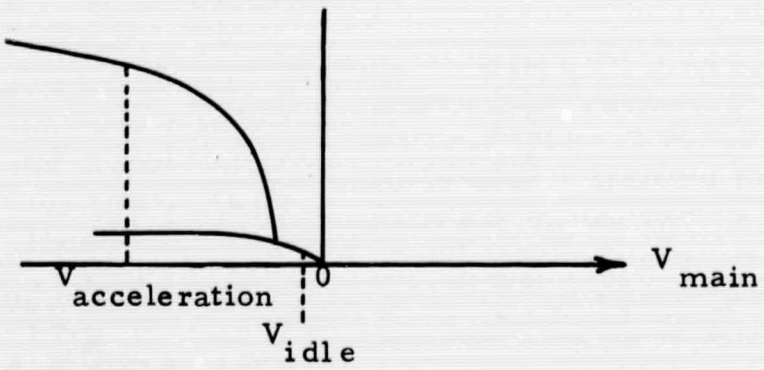

Figure 3. I-V Curve

64-R-2-5

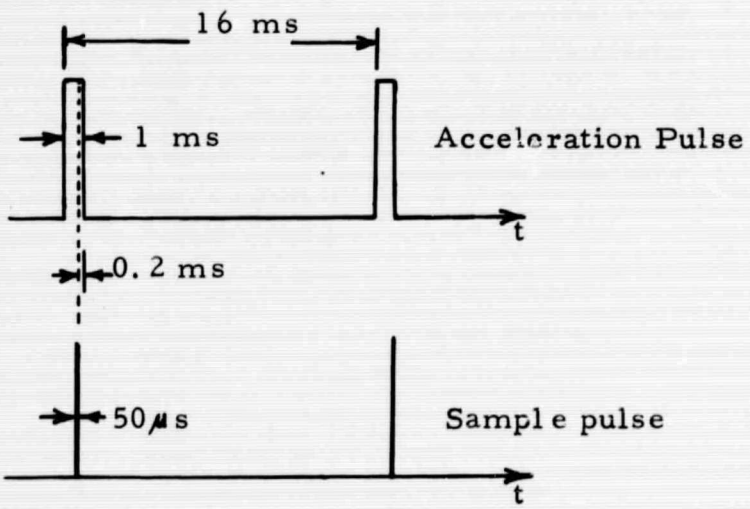

Figure 4. Pulse Timing

64-R-2-6

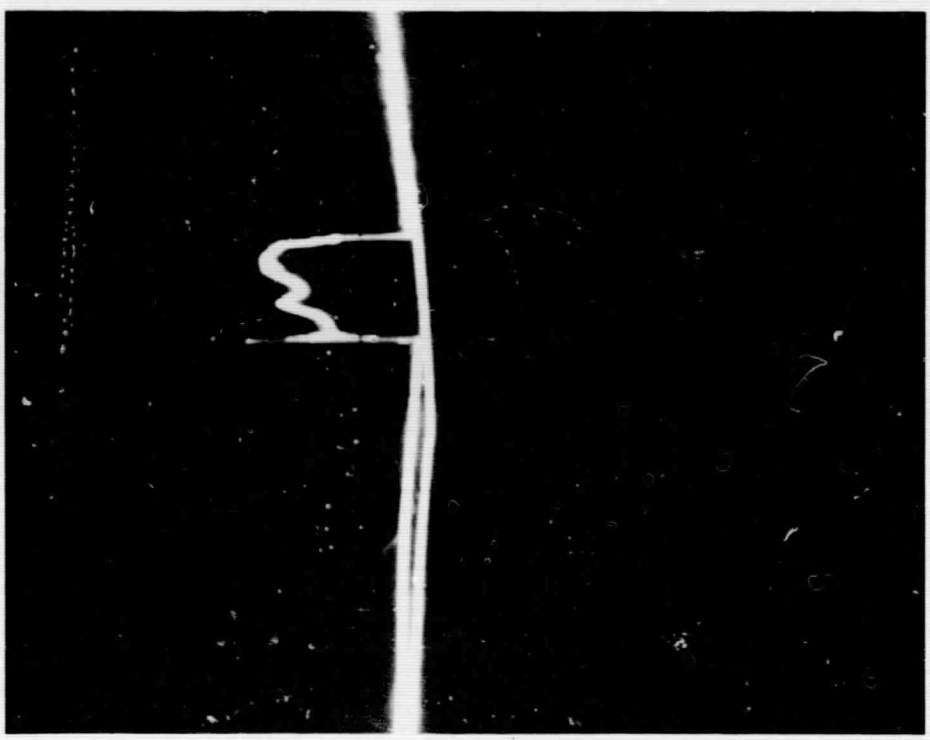

Figure 5. Pulse Cross-scan

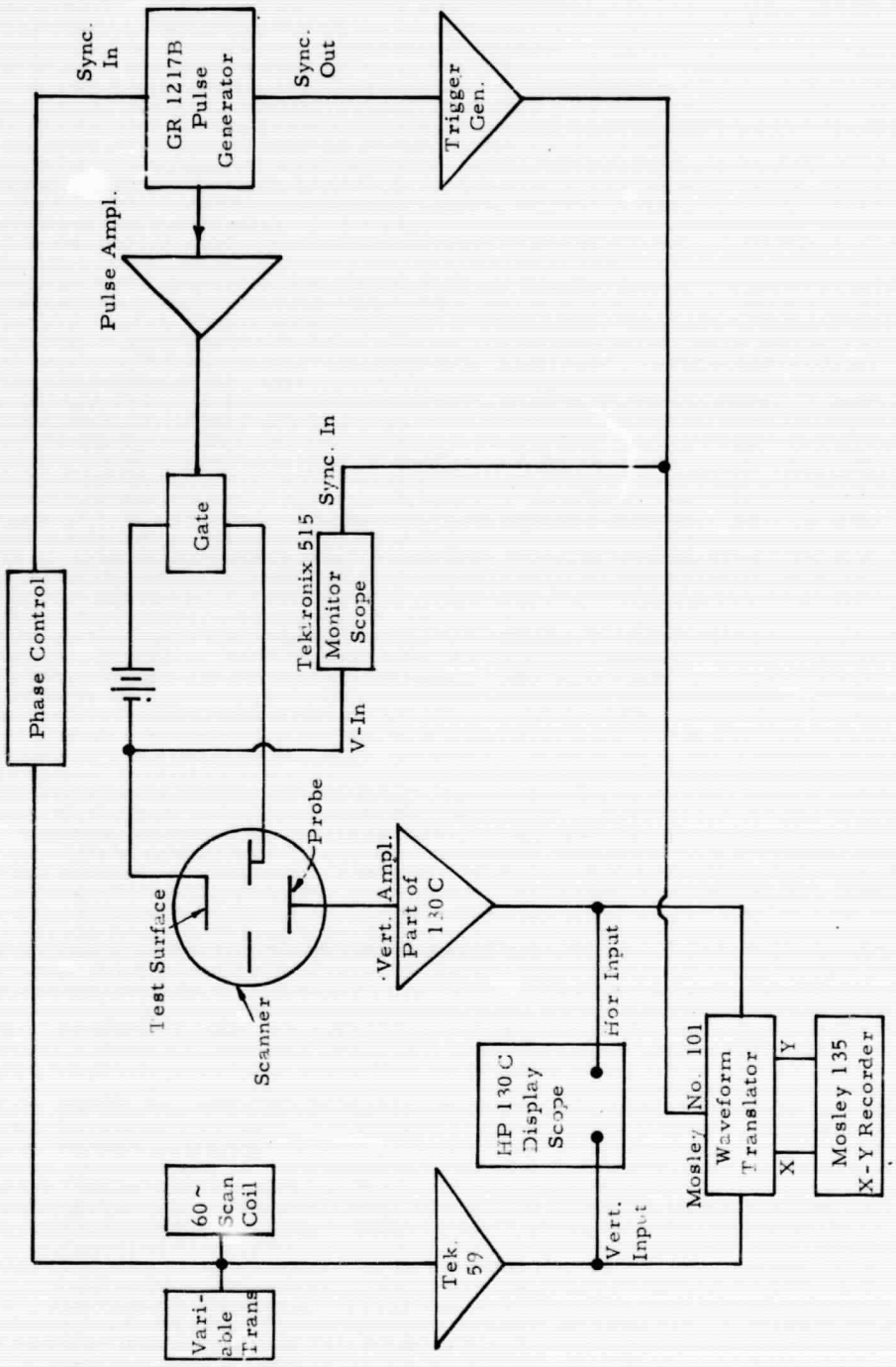

64-R-2-7

Figure 6 Schematic of Pulse System

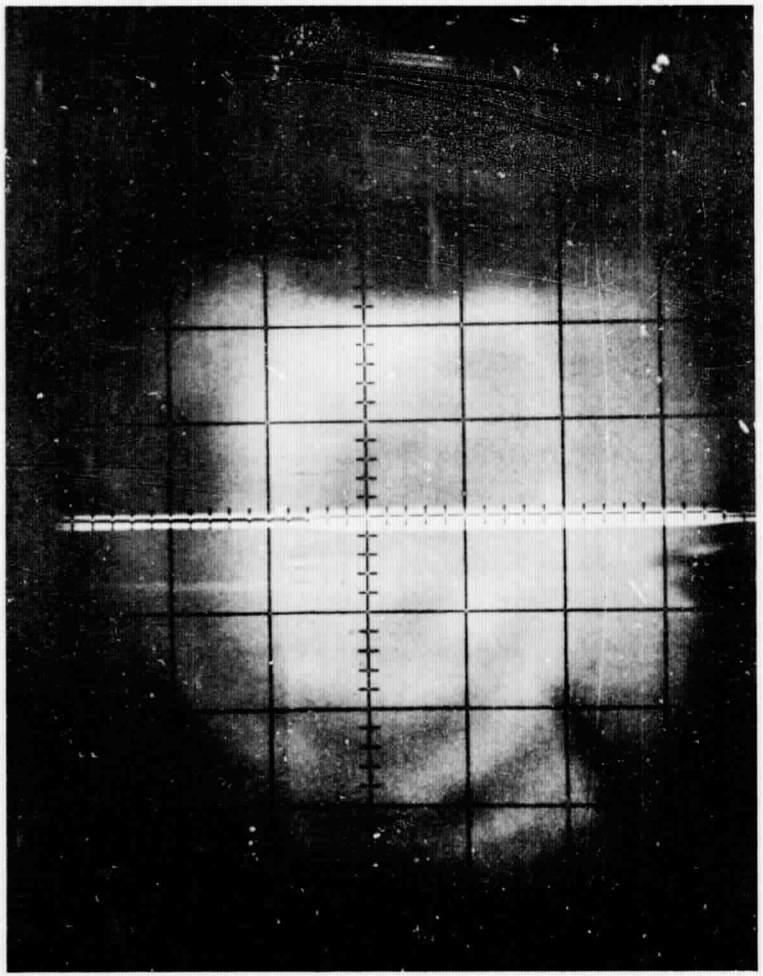

Figure 7 Display Photo (No. 6)

$T = 1280°K$, $T_R = 425°K$

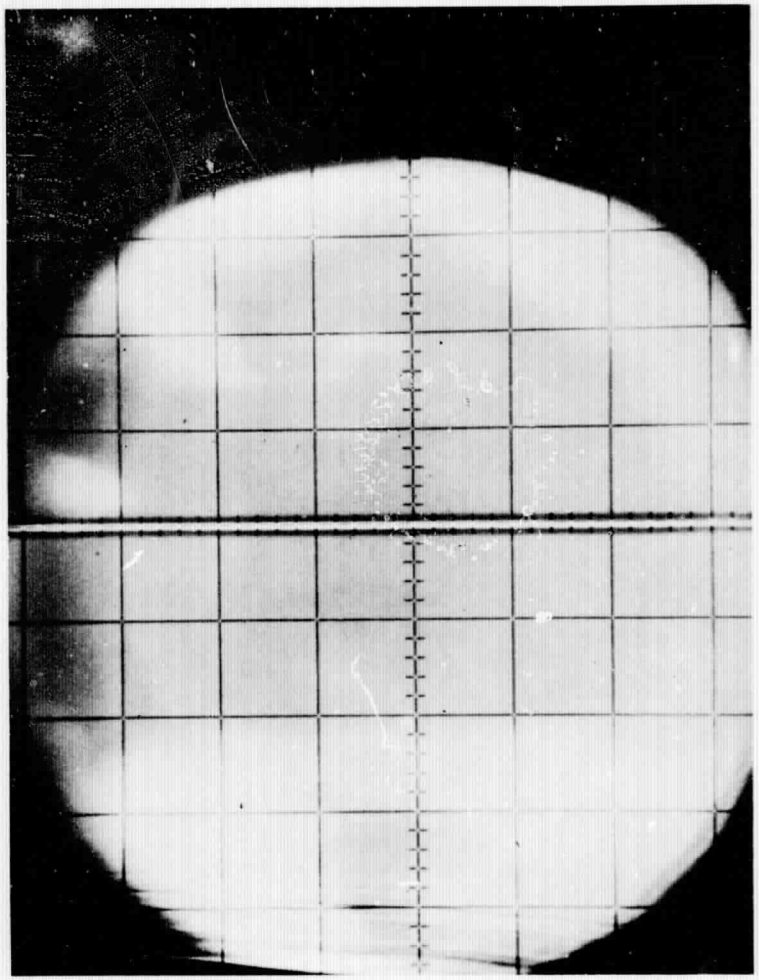

Figure 8. Display Photo (No. 12)

$T = 1280°K$, $T_R = 425°K$, $T_A = 425°K$

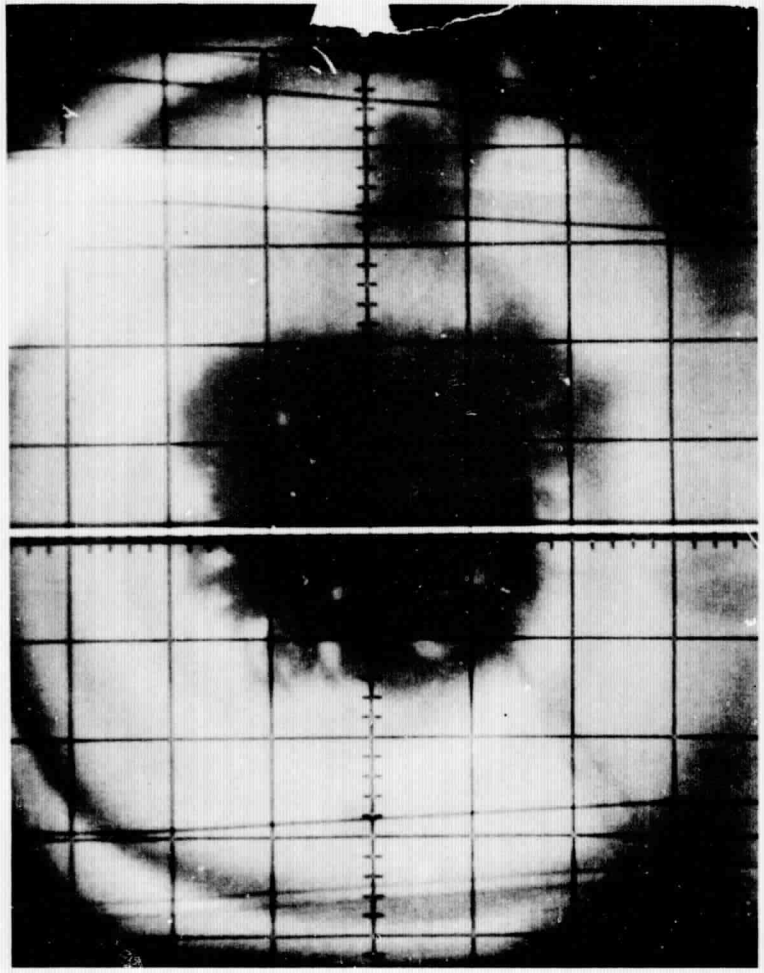

Figure 9. Display Photo (No. 21)

$T_{\cdot} = 1280°K$, $T_R = 425°K$, $T_A = 520°K$

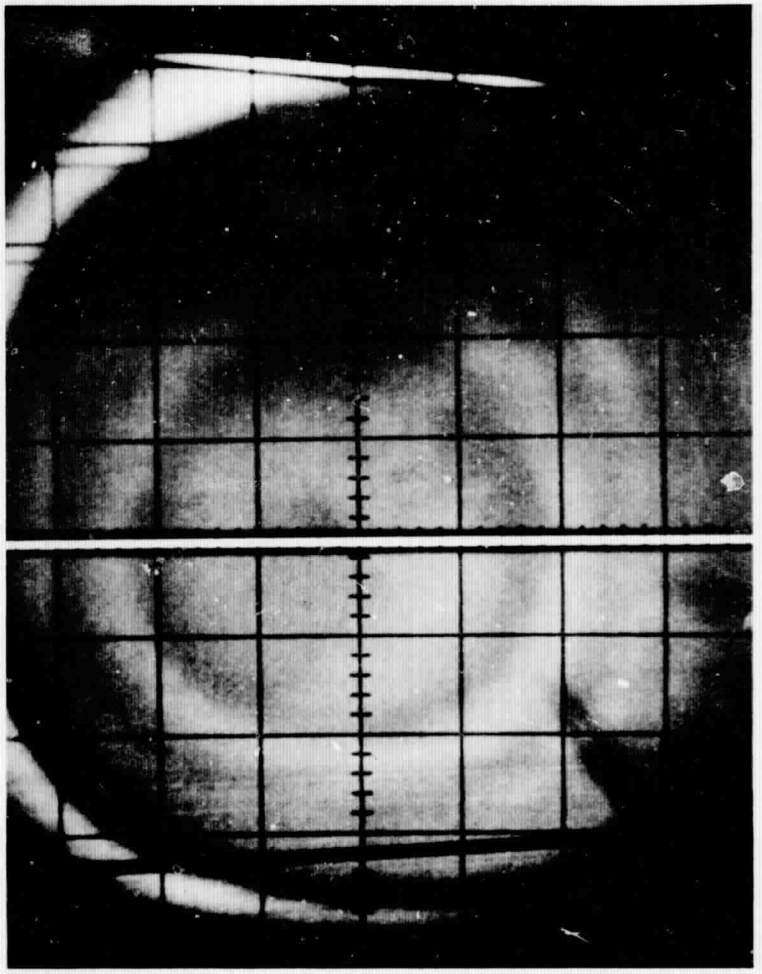

Figure 10. Display Photo (No. 19)

$T_{\cdot} = 1080°K$, $T_R = 425°K$, $T_A = 425°K$

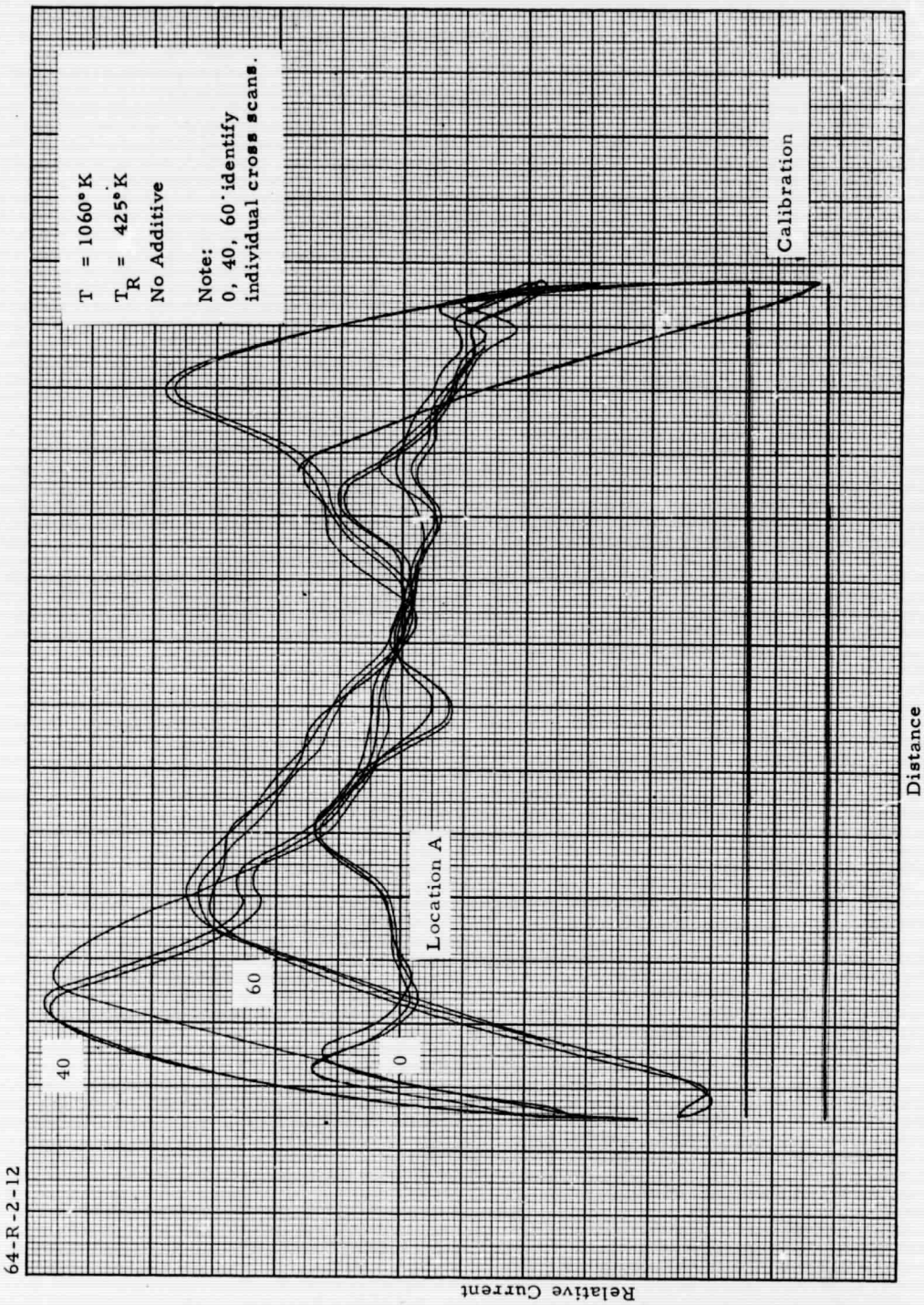

Figure 11. Cross Scan (No. 55) T = 1060° K, T_R = 425° K

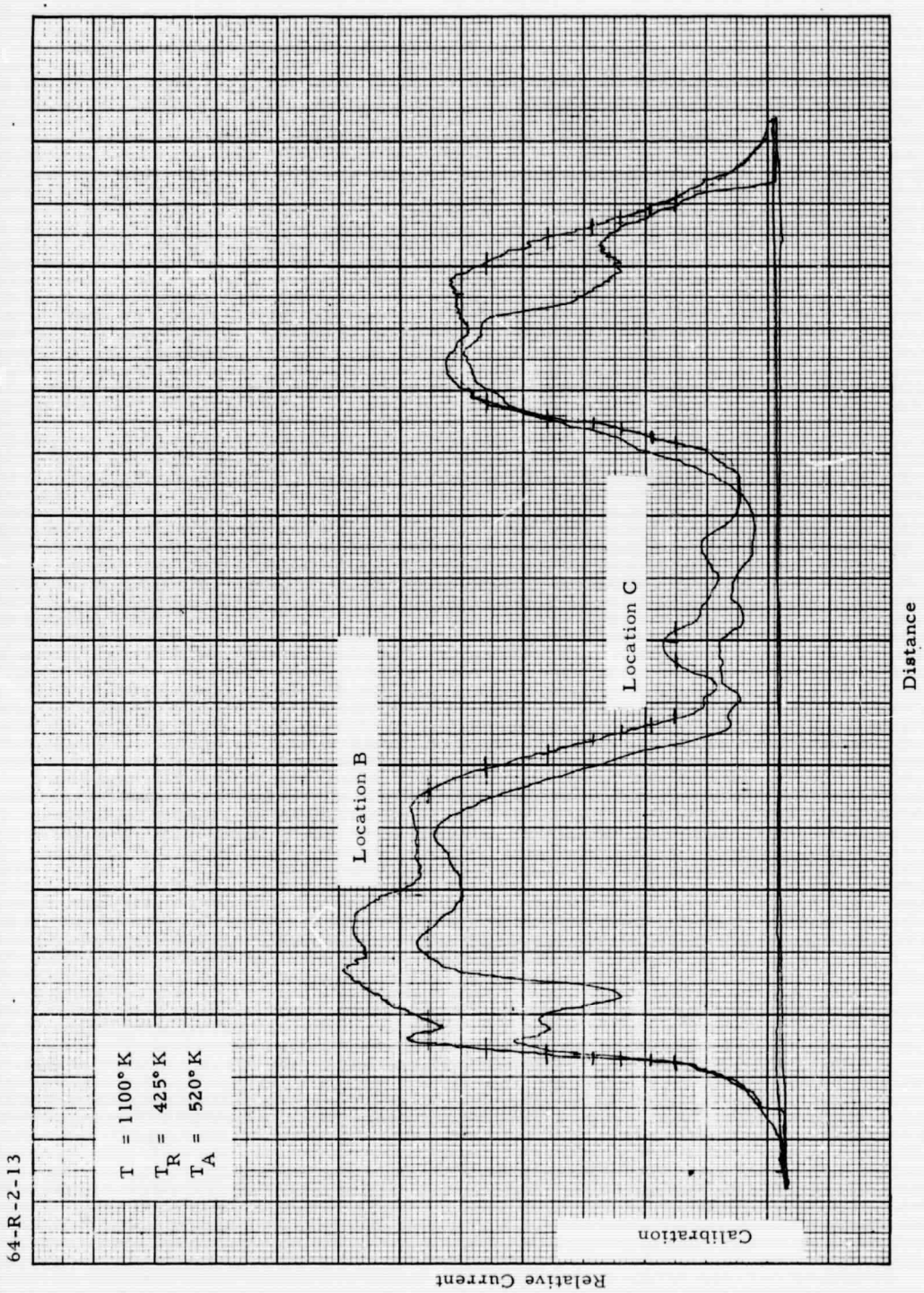

Figure 12. Cross-scan (No. 99) T = 1100°K, T_R = 425°K, T_A = 520°K

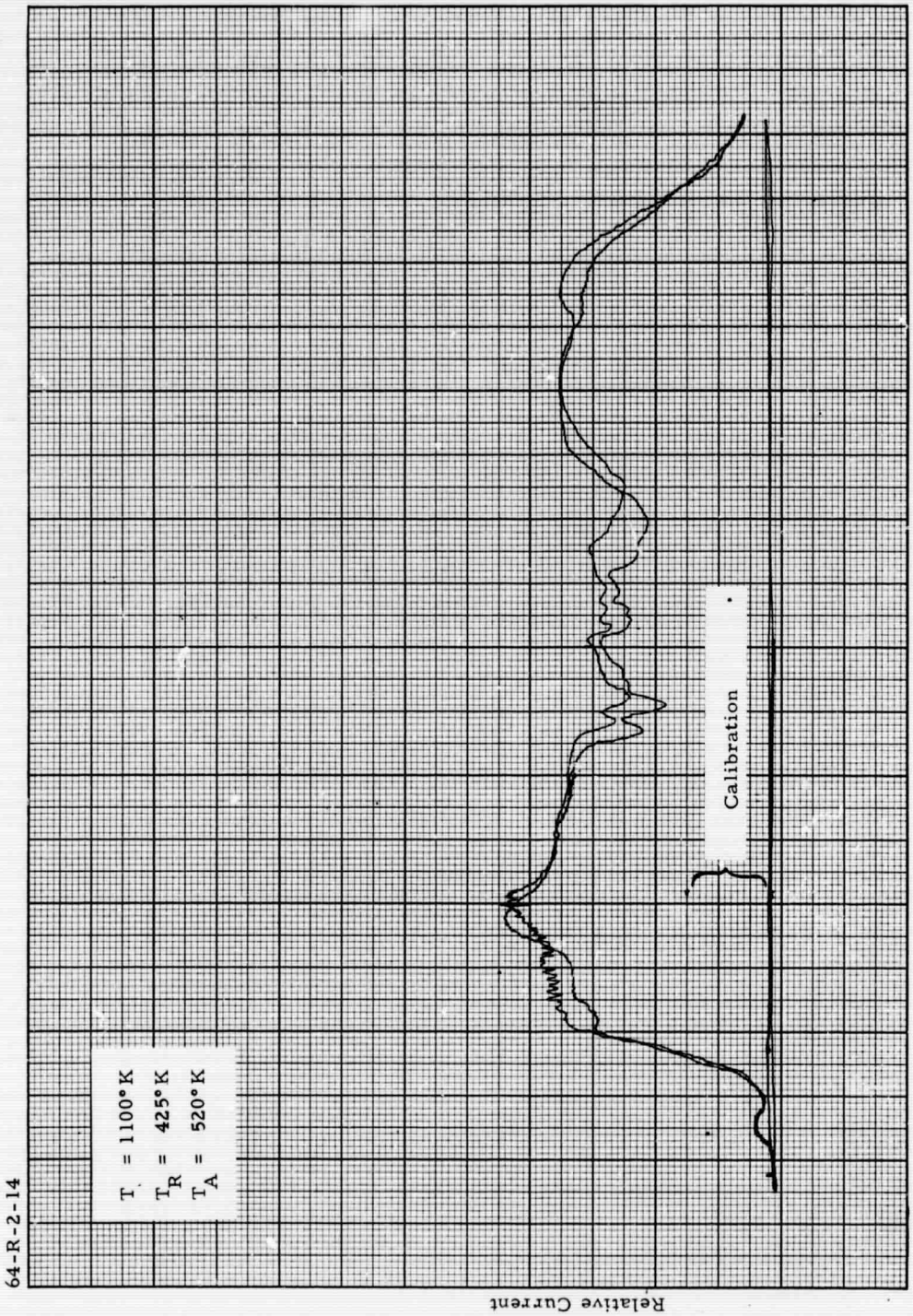

Figure 13. Cross-scan (No. 113) T = 1100°K, T_R = 425°K, T_A = 520°K

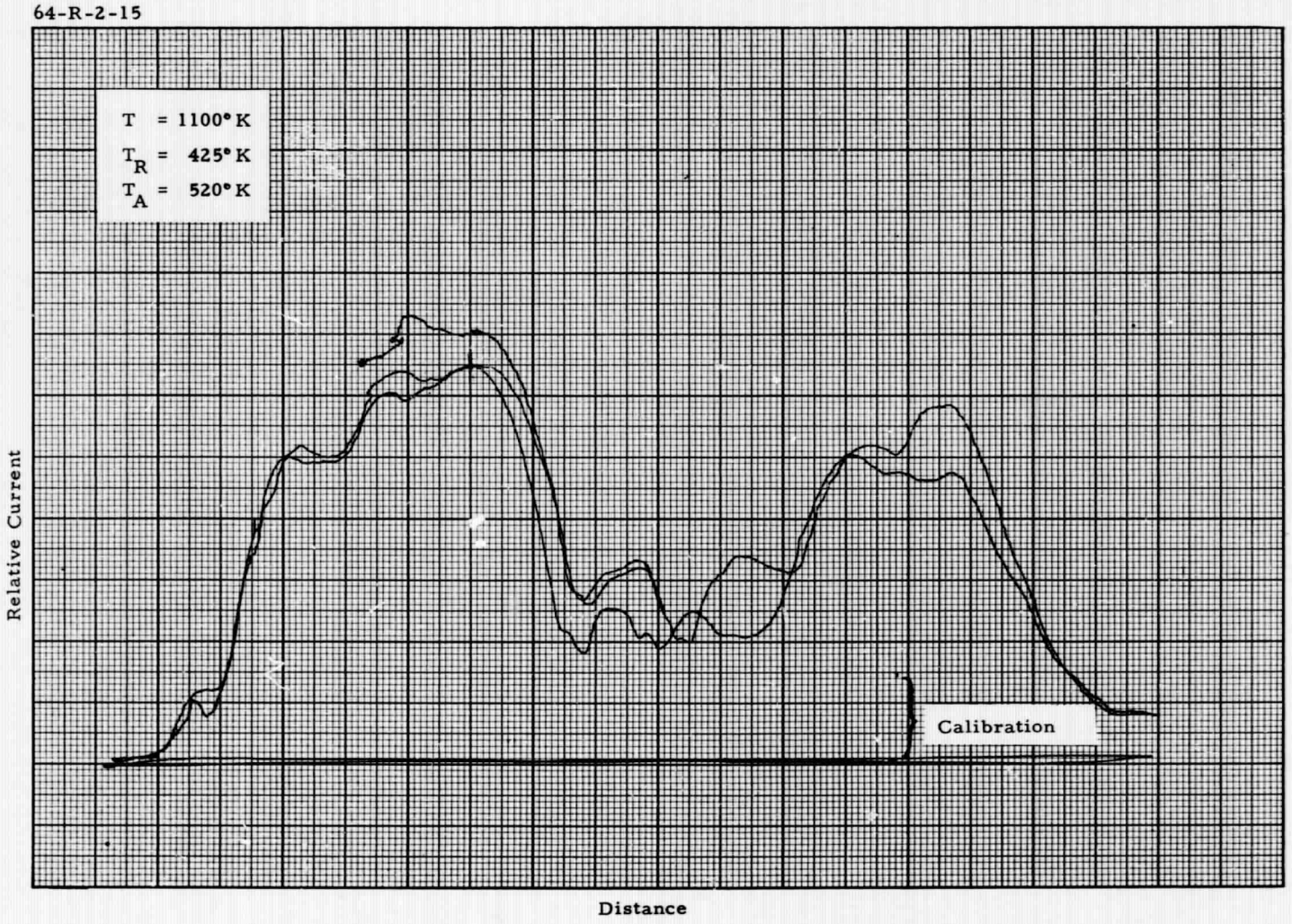

Figure 14. Cross-scan (No. 119) T = 1100°K, T_R = 425°K, T_A = 520°K

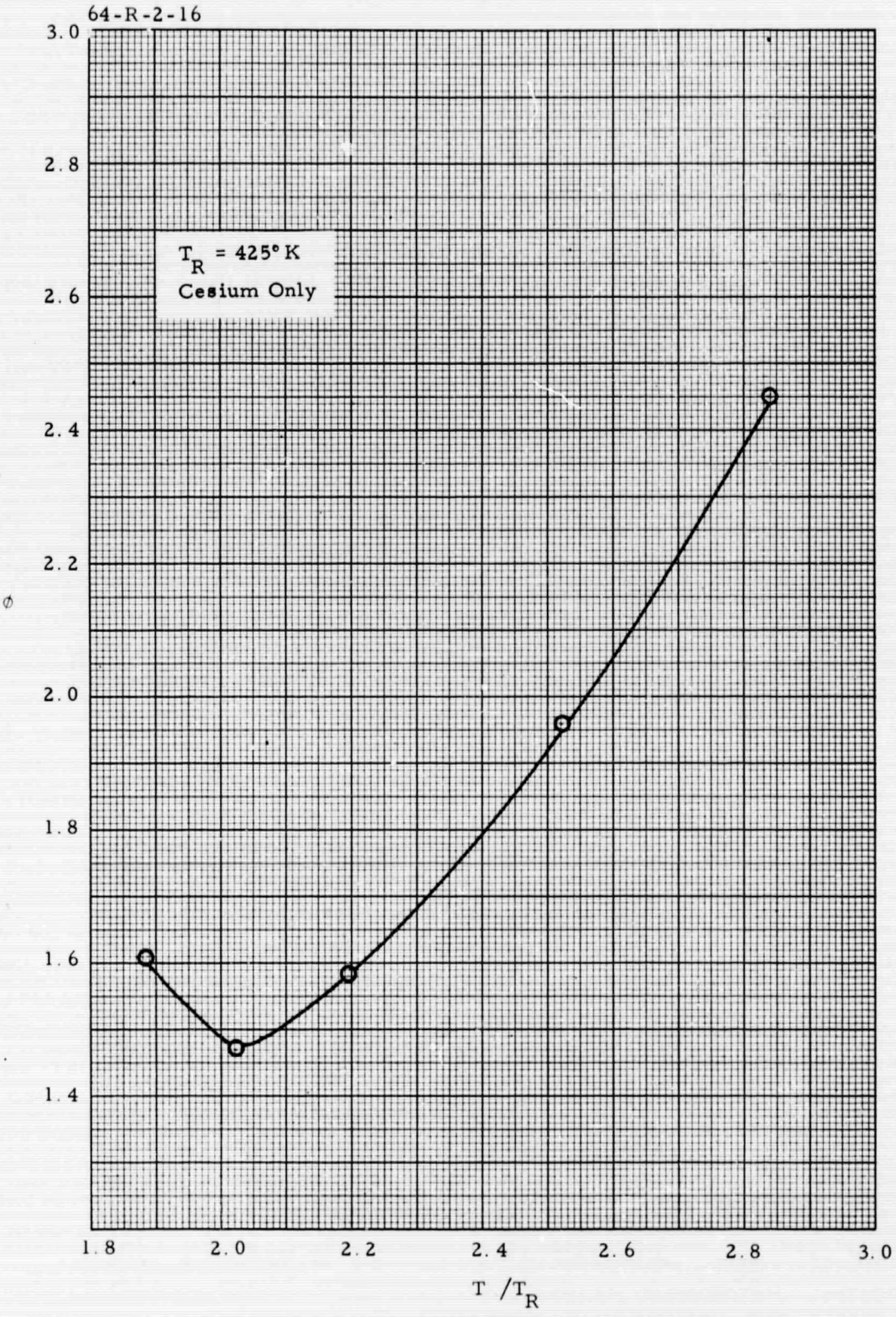

Figure 15. ϕ vs T /T_R, T_R = 425° K

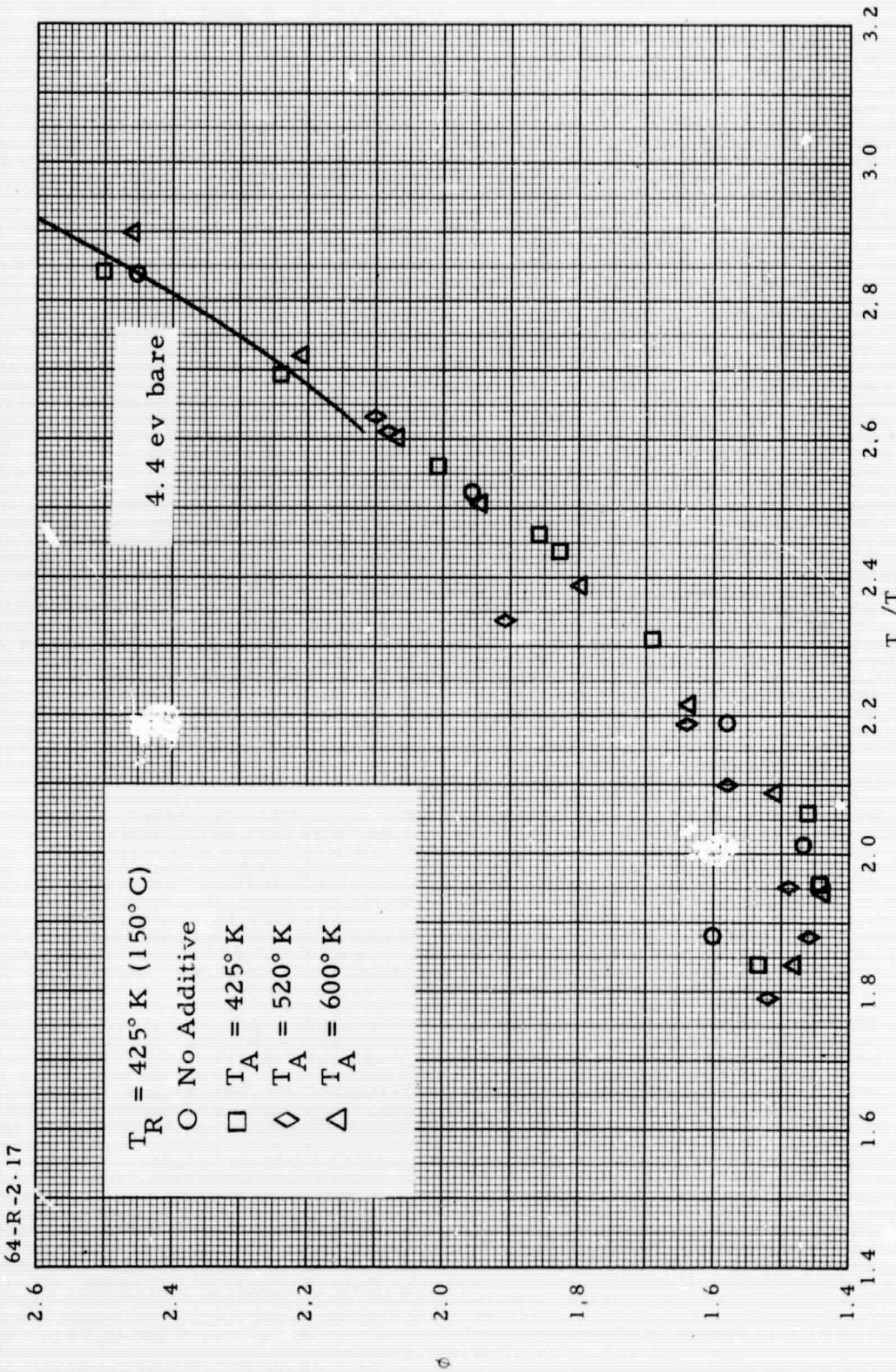

Figure 16. ϕ vs T/T_R, T_R = 425° K

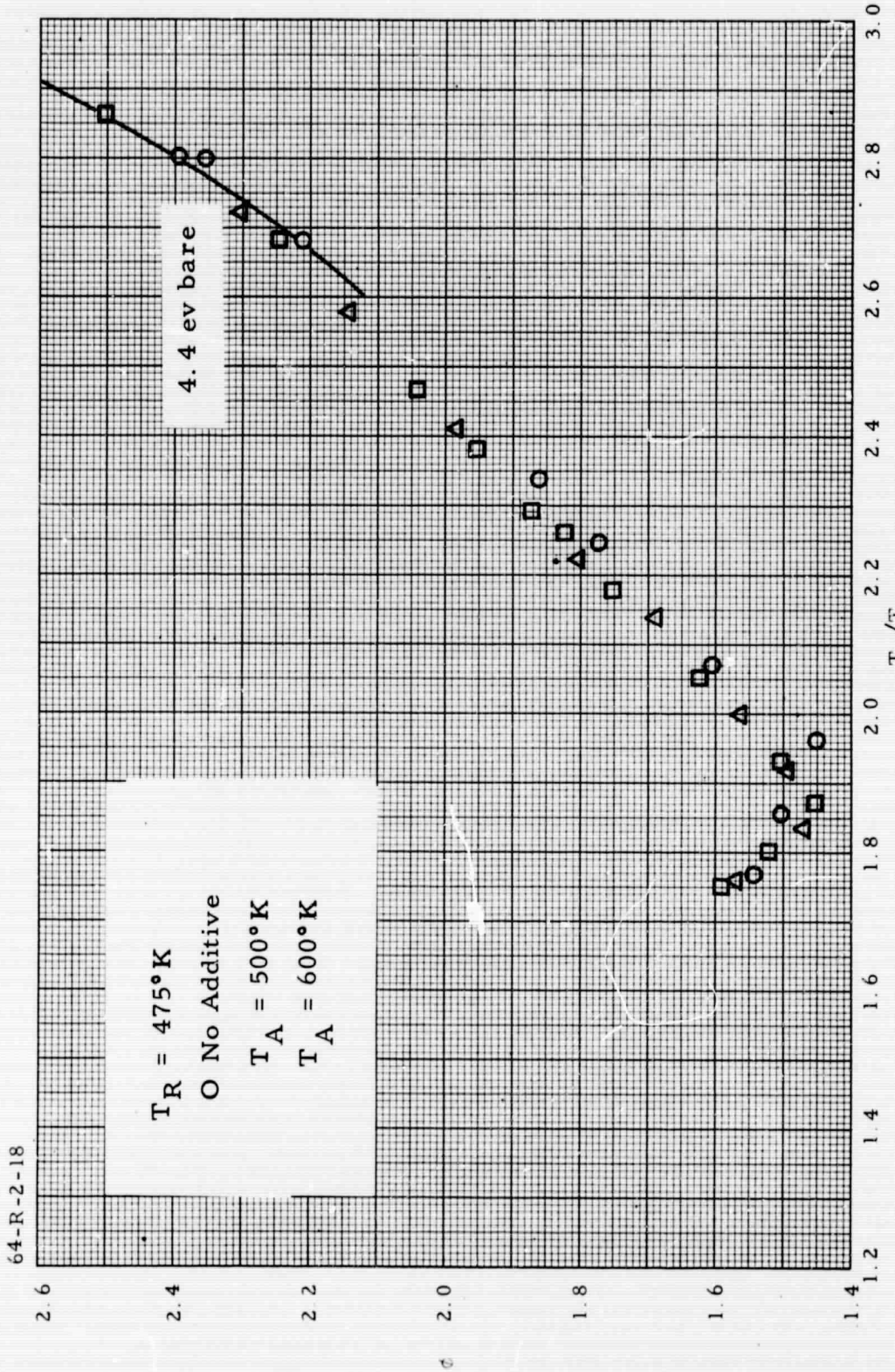

Figure 17 ϕ vs T/T_R, T_R = 475°K

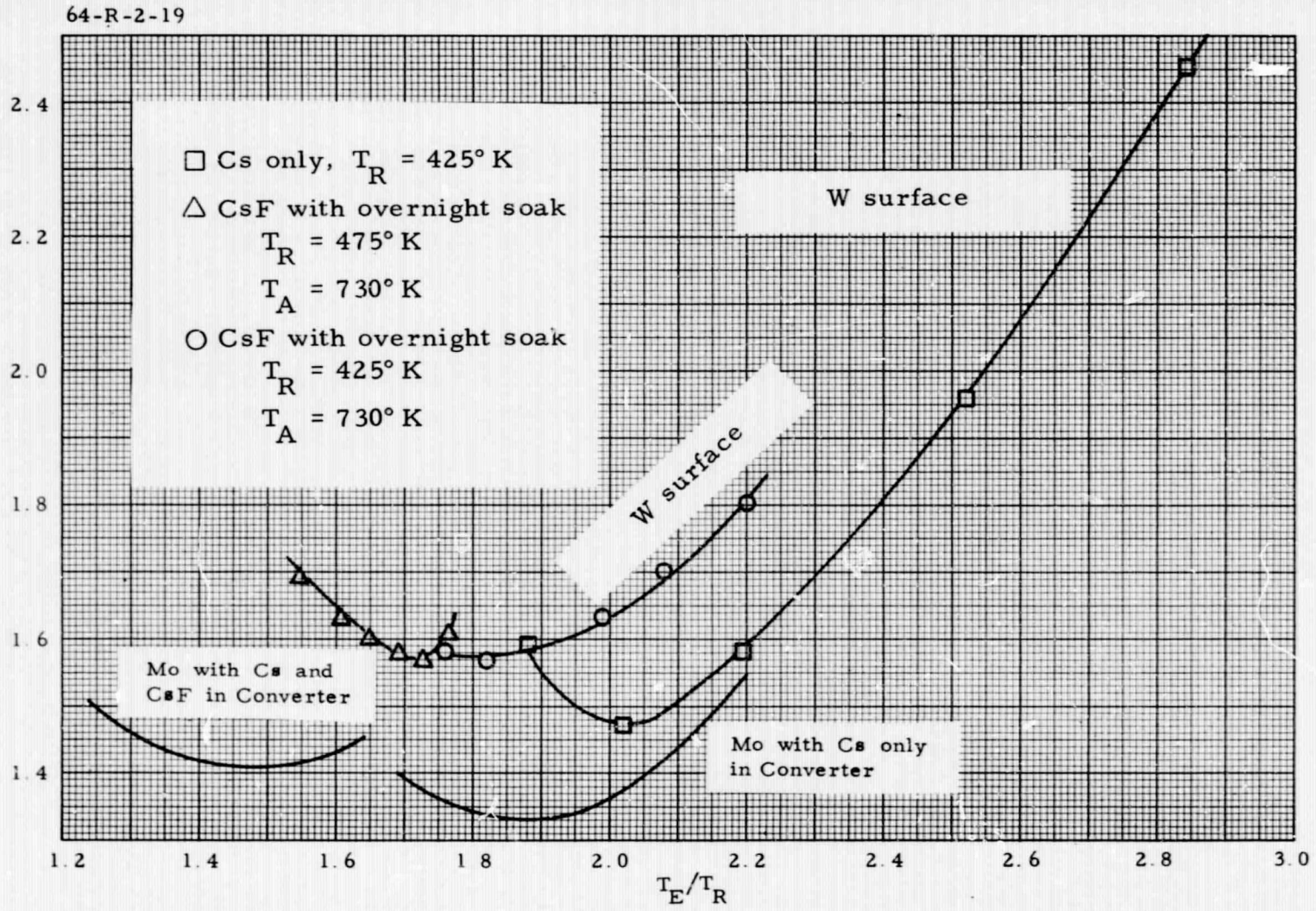

Figure 18. ϕ vs T_E/T_R Showing Effect of Additive

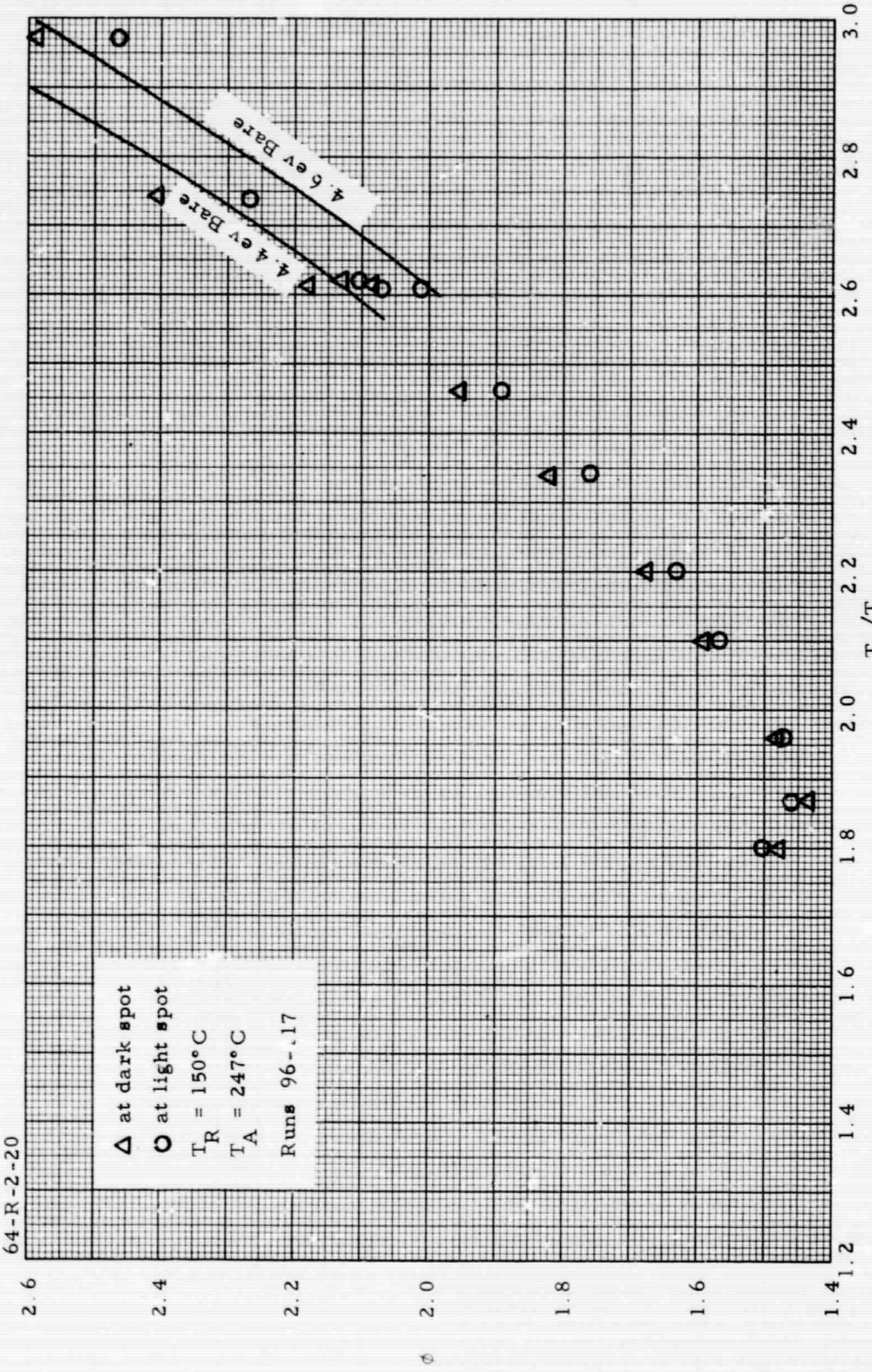

Figure 19. Work Function Plots of Two Patches

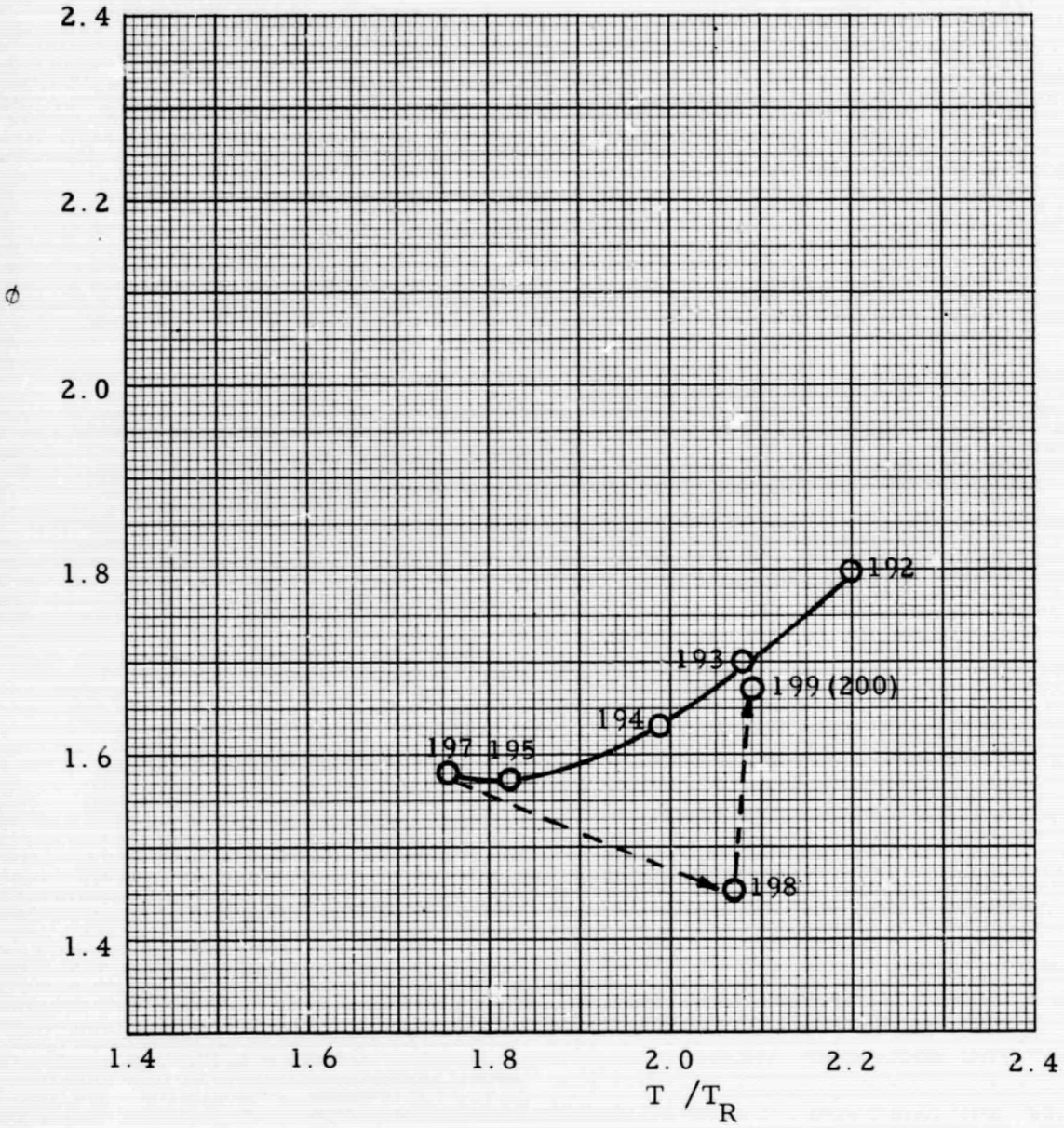

Figure 20. Time Effect With Additive